ZONGHE DIANZI XITONG JISHU
JIAOYUBU ZHONGDIAN SHIYANSHI
2011XUESHU NIANHUI

综合电子系统技术教育部重点实验室

2011学术年会

主　审　田　忠
主　编　张　伟　张顺生
副主编　甘　泉　张　可
　　曹建蜀　宗竹林

电子科技大学出版社

目　　录

一、雷达与电子战领域

二、通信、导航与传感器网络领域

三、其他领域

一、雷达与电子战领域

An Echo Simulation Algorithm in Terms of Equivalent Scatterer

Zhang Shunsheng
(Research Institute of Electronic Science and Technology,
University of Electronic Science and Technology of China, Chengdu 611731)

Abstract An echo simulation algorithm in terms of equivalent scatterer (ESA-ES) is presented. It is based on the model of equivalent scatterer for the scene, the approximate expression of synthetic aperture radar (SAR) system's impulse response function, and one-dimensional fast Fourier transform (FFT) for data processing. The effect of error with slant range approximation on echo simulation and imaging processing is analyzed. The performances of different echo simulation algorithms are drawn a comparison between the computational quantities and the simulation precision. Through numerical simulation of point target and natural scene, it is indicated that when SAR system contains the time-variant motion error, the ESA-ES algorithm can not only generate raw data fast, but ensure the simulation precision of echo data.

Key words echo simulation; equivalent scatterer; slant range approximation; simulation speed; simulation precision

1 Introduction

The simulation technology is an important means of scheme design, parameter optimization and system development of the complicated electronic system. The success of the applied systems of airborne or space-borne SAR cannot depart from the support of it. In order to ensure that the designed SAR systems satisfy the specific requirements of different users, raw data simulation and imaging processing are implemented before the development of SAR system. In addition, large amounts of echo data will be needed in the process of ground imaging system. Therefore, SAR raw data simulation. is a significant component of SAR simulation technology.

The comparatively typical echo simulation algorithms of SAR include a range time-domain pulse coherence (RTPC) algorithm, a two-dimensional frequency domain Fourier transform (2D FFT) algorithm and an imaging inverse processing (IMIP) algorithm according to the references.

The principle of RTPC is to generate echo signal through the convolution of the transmitting signal and impulse response function of SAR system. However, some errors are introduced in order to make target's echo fell on the integral sampling dot, as reduces the simulation precision of echo signal. 2D FFT was first proposed by an Italian named Franceschetti. It was realized by multiplying the two-dimensional spectrum of targets' scattering characteristic and two-dimensional frequency-domain expression of SAR system transfer function, then the time-domain echo signal is gotten by 2D inverse Fourier transform. Comparing with

the RTPC algorithm, the operation efficiency of this algorithm is improved distinctly. However, when the motion errors or attitude errors of the radar platform exist, the motion track and beam point direction can not be used in the frequency-domain expression of system transfer function. As a result, 2D FFT is restricted by both the platform's motion errors and the antenna's attitude errors. IMIP is to transform image data into signal space by inverse imaging processing, then the simulated echo signal is obtained. This algorithm includes RD (Range-Doppler) inverse processing algorithm and wave-number domain inverse processing algorithm, whose efficiency is higher than that of RTPC. However, it is also limited by the time-variant velocity errors and the attitude dithering errors. When SAR system contains these errors, the simulated echo signal is imprecise.

In order to compromise between computation efficiency and simulation precision, an echo simulation algorithm in terms of equivalent scatterer (ESA–ES) is presented in this paper.

2 The Echo Simulation Algorithm in Terms of Equivalent Scatterer

2.1 The Principle

The established slant plane coordinate system is shown in Fig. 1. The Y-axis represents the motion direction of the platform, the R-axis denotes the slant range direction orthogonal to the Y-axis, O_r is the centre of the slant plane coordinate system. Assumed that the coordinate of the radar platform is $(0, y(t_a))$ at t_a time, the minimum distance from the radar platform to the target scene is $r_{\min}$. The simulated natural scene is composed of large numbers of point targets distributed on the rectangle grid. The interval of the adjacent rectangle grid along the Y direction is Δy , and the interval along the R direction is Δr . Supposed that the targets' backscattering coefficients of natural scene are described by a two-dimensional matrix, that is

$$\boldsymbol{\sigma} = [\sigma_{mn}]_{M\times N} \tag{1}$$

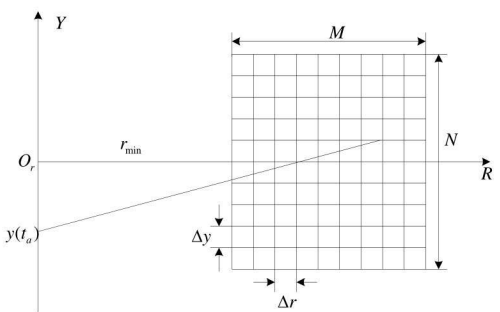

Fig. 1 The geometric relation of the slant plane

In (1), M, N represents the grid number along the R and Y direction respectively, σ_{mn} denotes the target's backscattering coefficient of the (m,n) grid.

So, the echo signal of natural scene can be expressed as[9]

$$s_r(t_r,t_a)=\sum_{m=1}^{M}\sum_{n=1}^{N}\sigma_{mn}\exp\left(-j\frac{4\pi R_{mn}(t_a)}{\lambda}\right)\cdot a\left(t_r-\frac{2R_{mn}(t_a)}{c}\right)\cdot \exp\left[j\pi\gamma\left(t_r-\frac{2R_{mn}(t_a)}{c}\right)^2\right] \tag{2}$$

where t_r denotes the fast-time, t_a represents the slow-time, λ is the wavelength, c is the speed of light, $a(t_r)$ is the rectangular window, γ is the slope of linear frequency modulated signal, $R_{mn}(t_a)$ is the distance between the target of the (m,n) grid and the radar platform.

$$R_{mn}(t_a)=\sqrt{(r_{\min}+m\cdot\Delta r)^2+(y(t_a)-n\cdot\Delta y)^2} \quad (3)$$

Assumed that point targets on rectangle grid can be considered as distributing in large numbers of equal range rings that virtually exist, which is shown in Fig. 2.

Provided that the interval of equal range ring is Δsp, the maximum distance from the radar platform to the target scene is $r_{\max}$. Then, the number of equal range ring is

$$n_e=\mathrm{int}\left[\frac{r_{\max}-r_{\min}}{\Delta sp}\right]+1 \quad (4)$$

The initial distance of the sampling window is

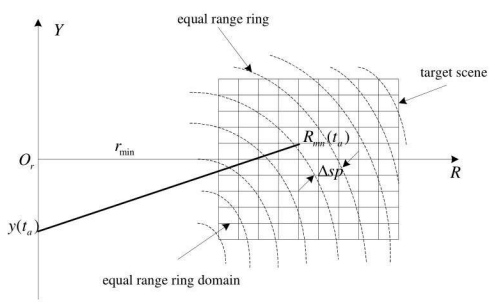

Fig. 2 The sketch map of the equal range ring

$$R_{\min}=\mathrm{int}\left[\frac{r_{\min}}{\Delta sp}\right]\cdot\Delta sp-\frac{\Delta sp}{2} \quad (5)$$

Then, the target's slant range in the (m,n) grid meets the following inequality

$$\begin{aligned}R_{\min}(t_a)+(p-1)\Delta sp &\le R_{mn}(t_a)\\ &< R_{\min}(t_a)+p\cdot\Delta sp\\ p&\in[1,n_e]\end{aligned} \quad (6)$$

The above inequality implies that point targets on the rectangle grid fall within any adjacent equal range ring. With regard to the p-th equal range ring domain, the range of m,n can be determined via solving the above inequality

$$\begin{aligned}m&\in[m_1,m_2] \quad m_1,m_2\in[1,M]\\ n&\in[n_1,n_2] \quad n_1,n_2\in[1,N]\end{aligned} \quad (7)$$

In order to calculate the backscattering coefficients of all targets in the p-th equal range ring domain, we analyze the targets' distribution (see Fig. 3).

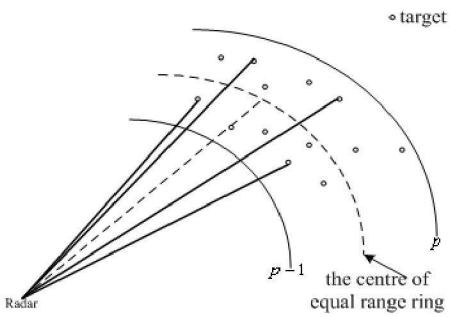

Fig. 3 Targets' distribution of the adjacent equal range ring domain

In Fig. 3, $p-1$ and p represent the adjacent two equal range rings, and the distances from them to the radar are $R_{\min}(t_a)+(p-1)\Delta sp$, $R_{\min}(t_a)+p\cdot\Delta sp$ respectively. The distance between the centre of the adjacent equal range ring and the radar is $R_{\min}(t_a)+(p-\frac{1}{2})\Delta sp$. The approximation is adopted that the distances from the targets in the adjacent equal range ring domain to the radar are replaced with the slant range of the equal range ring's centre in order to compute backscattering coefficients. Accordingly, all targets in this domain are referred to as the equivalent scatterer, whose backscattering coefficient is expressed as

$$\sigma_p=\sum_{m=m_1}^{m_2}\sum_{n=n_1}^{n_2}\sigma_{mn}\exp\left(-j\frac{4\pi\Delta r_{mn}(t_a)}{\lambda}\right) \quad (8)$$

In (8), $\Delta r_{mn}(t_a)$ denotes the difference of slant range between the target in the (m,n) grid and the equal range ring's centre

$$\begin{aligned}\Delta r_{mn}(t_a)&=R_{mn}(t_a)-\left(R_{\min}(t_a)+(p-\frac{1}{2})\Delta sp\right)\\ p&\in[1,n_e]\end{aligned} \quad (9)$$

Equation (8) and (9) are used in (2), and the slant range of the equal range ring's centre is substituted for $R_{mn}(t_a)$ of latter two items in (2). Then, the echo signal of natural scene is written as

$$s_r(t_r,t_a)=\sum_{p=1}^{n_e}\sigma_p \exp\left[-j\frac{4\pi\left(R_{\min}(t_a)+(p-1/2)\Delta sp\right)}{\lambda}\right] a\left[t_r-\frac{2\left(R_{\min}(t_a)+(p-1/2)\Delta sp\right)}{c}\right]\cdot \exp\left[j\pi\gamma\left(t_r-\frac{2\left(R_{\min}(t_a)+(p-1/2)\Delta sp\right)}{c}\right)^2\right] \quad (10)$$

The constraints are

$$R_{\min}(t_a)+(p-1)\Delta sp \leqslant R_{mn}(t_a) < R_{\min}(t_a)+p\cdot\Delta sp$$
$$p\in[1,n_e]$$
$$1\leqslant m\leqslant M$$
$$1\leqslant n\leqslant N \quad (11)$$

It is noted that the latter two items of (10) are only related to the fast-time variable t_r. Accordingly, equation (10) can also be written in the following convolution format.

$$s_r(t_r,t_a)=a(t_r)\exp(j\pi\gamma t_r^2)\otimes_{t_r}\sum_{p=1}^{n_e}\sigma_p\cdot \exp\left[-j\frac{4\pi\left(R_{\min}(t_a)+(p-1/2)\Delta sp\right)}{\lambda}\right]\cdot \delta\left[t_r-\frac{2\left(R_{\min}(t_a)+(p-1/2)\Delta sp\right)}{c}\right] \quad (12)$$

where $\otimes_{t_r}$ represents the convolution versus fast-time. The physical meanings of the above equation is that the received signal is the response of a linear time-invariant system, the system input is the base-band linear frequency modulated signal and the output is the result of convolution between the transmitting signal and the impulse response function with a certain amplitude, phase and delay.

In digital signal processing, the fast convolution can be implemented by FFT.

2.2 The Simulation Procedures

According to the principle of the ESA–ES algorithm, the procedures of generating natural scene's echo data are as follows.

a. Set system simulation parameters and input the targets' backscattering coefficients of natural scene.

b. Generate the transmitting signal and compute its FFT.

c. Calculate the minimum and maximum distance from the radar platform to target scene, and determine the numbers of equal range ring.

d. Compute the equivalent scatterer's backscattering coefficient in the adjacent equal range ring domain, and get the system's impulse response function and its FFT.

e. Multiply d by b, transform their product into time domain and get a pulse's echo signal.

f. In terms of pulse order in azimuth direction repeat (d)～(e) procedure, raw echo data of natural scene can be simulated.

3 Error Analysis

In order to calculate the equivalent scatterer's backscattering coefficient in the adjacent equal range ring domain, the slant ranges from all targets in the domain to the radar platform are regarded as the distance between the adjacent equal range ring's centre and the platform. The slant range approximation inevitably brings errors to echo

simulation and imaging processing.

Taking point target as example, the effect of slant range approximation on echo simulation and imaging processing is analyzed from the angle of mathematical formula and numerical simulation.

3.1 The Effect of Slant Range Approximation on Echo Simulation

At a certain pulse time t_a, assumed that there is a point target in the adjacent equal range ring domain, the distance from the target to the phase centre of the antenna is $R(t_a)$, and σ is its backscattering coefficient. The distance between the adjacent equal range ring's centre and the radar platform is $R_m(t_a)$. The difference of slant range from the target to the adjacent equal range ring's centre is Δr. Then, the equivalent scatterer's backscattering coefficient is

$$\sigma_e = \sigma \cdot \exp\left(-j\frac{4\pi\Delta r}{\lambda}\right) \tag{13}$$

In order to simplify the following analysis, supposed that σ is equal to 1. Then, according to the model of slant range approximation, the equivalent scatterer's echo signal is given by

$$s_e(t_r,t_a) = a\left(t_r - \frac{2R_m(t_a)}{c}\right)\cdot \exp\left[j\pi\gamma\left(t_r - \frac{2R_m(t_a)}{c}\right)^2\right]\cdot\exp\left(-j\frac{4\pi R(t_a)}{\lambda}\right) \tag{14}$$

Without the approximate model, the echo signal of the actual target is

$$s(t_r,t_a) = a\left(t_r - \frac{2R(t_a)}{c}\right)\cdot \exp\left[j\pi\gamma\left(t_r - \frac{2R(t_a)}{c}\right)^2\right]\cdot\exp\left(-j\frac{4\pi R(t_a)}{\lambda}\right) \tag{15}$$

In (14) and (15), the first item is the envelop of echo signal, the second and the third item are the Chirp and Doppler component respectively. From these two equations, it can be seen that their echo envelops and Chirp components are different while Doppler components are the same. This is because the delays of actual target and equivalent scatterer are different. It also illustrates that the slant range approximation mainly results in the error of echo signal envelop and pulse-inside phase.

As is known that the envelop migration cannot exceed half of range resolution cell usually. So, the difference of slant range between the actual target and the equivalent scatterer must satisfy

$$\Delta r \leqslant \frac{1}{2}\cdot\frac{c}{2B} \tag{16}$$

where B is the signal bandwidth.

In fact, in order to make target's location fell on the integer sampling point, the interval of the adjacent equal range ring must meet

$$\Delta sp = \frac{1}{n_{sp}}\cdot\frac{c}{2f_s} \tag{17}$$

In (17), f_s is the sampling rate, n_{sp} is the up-sampling times. In the following, the effect of the interval of the adjacent equal range ring on echo simulation is illustrated through numerical simulation.

Provided that the transmitting signal bandwidth is 150MHz, the sampling rate is 200MHz. Let the intervals of the adjacent equal range ring are equal to 1 times and 16-th of the sampling interval respectively, the amplitude and phase error of echo signal with slant range approximation versus echo signal with no approximation are shown in Fig. 4 and Fig. 5 respectively.

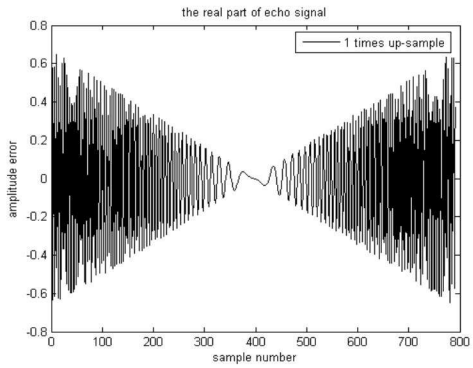

（a）Amplitude error

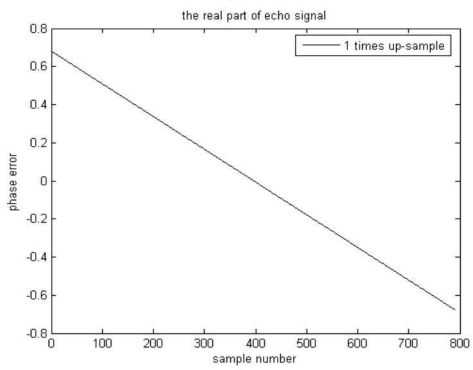

（b）Phase error

Fig.4 n_{sp}=1, the amplitude and phase error of echo signal with slant range approximation

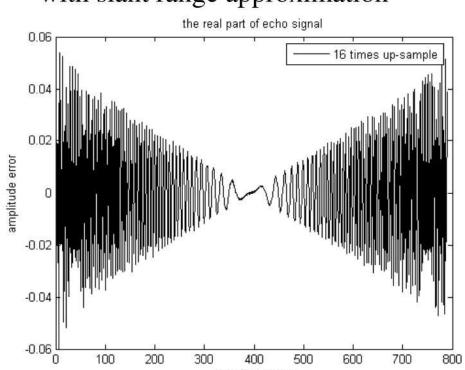

（a）Amplitude error

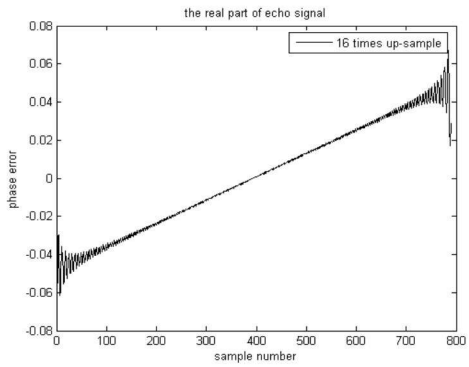

（b）Phase error

Fig.5 n_{sp}=16, the amplitude and phase error of echo signal with slant range approximation

From the simulation results, it can be shown that the amplitude and phase error of echo signal with slant range approximation reduces with the decrease of the interval of the adjacent equal rang ring. When the up-sampling times are equal to 16, the maximum amplitude error of echo signal with slant range approximation is 0.06 radian, and the maximum phase error is 0.06 radian, as can meet the requirement of echo simulation.

3.2 The Effect of Slant Range Approximation on Imaging Processing

SAR imaging is a process of two-dimensional correlation, which can be decomposed into two one-dimensional processing including range and azimuth processing.

Using (14), the matched filtering is performed in range dimension toward target's echo with slant range approximation. The compressed signal is

$$s_{re}(t_r,t_a)=\sqrt{BT_p}\cdot\sin c\left[B\left(t_r-\frac{2R_m(t_a)}{c}\right)\right]\cdot\exp\left(-j\frac{4\pi R(t_a)}{\lambda}\right) \quad (18)$$

The range processing is fulfilled toward target's echo without the approximation utilizing (15). The compressed signal is

$$s_{ra}(t_r,t_a)=\sqrt{BT_p}\cdot \sin c\left[B\left(t_r-\frac{2R(t_a)}{c}\right)\right]\cdot\exp\left(-j\frac{4\pi R(t_a)}{\lambda}\right) \quad (19)$$

where $\sin c(x)=\sin(\pi x)/(\pi x)$. According to the property of $\sin c$ function, the position of signal peak with slant range approximation is located at $2R_m(t_a)/c$, and the position with no approximation is $2R(t_a)/c$. That is, the position of the point target causes shift. The offset is determined by the following equation

$$n_r=\frac{\Delta r}{c/(2f_s)} \quad (20)$$

It is shown that the target's position offset cannot exceed half of range resolution cell. When the interval of the adjacent equal rang ring is very small, the effect of this offset can be neglected.

Point target's raw echo data with slant range approximation and with no approximation is generated respectively and imaging processing is performed toward echo data. The profiles of range and azimuth compression are shown in Fig. 6 and Fig. 7 respectively.

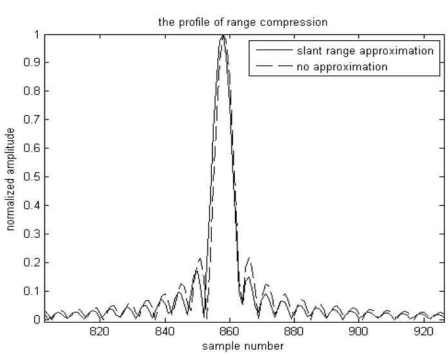

（a）The profile of range compression

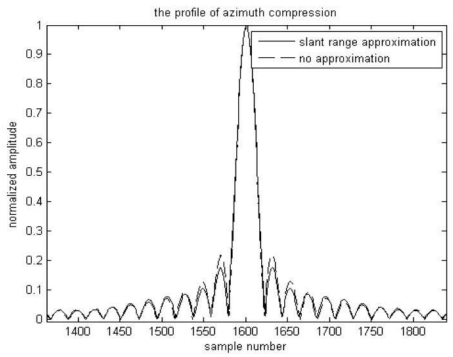

（b）The profile of azimuth compression

Fig. 6 n_{sp}=1, the profile of range and azimuth compression

(4 times interpolation)

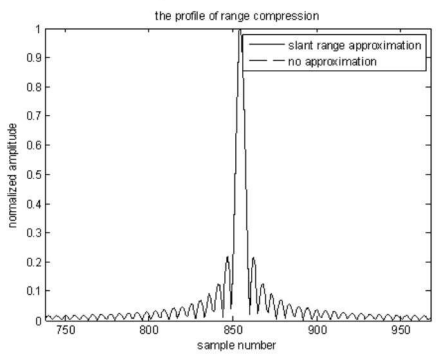

（a）The profile of range compression

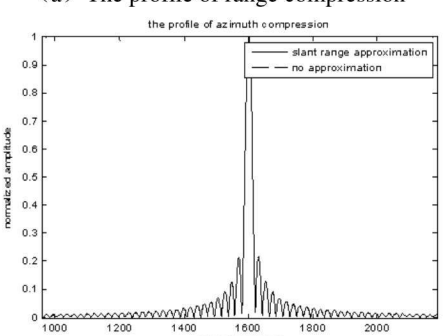

（b）The profile of azimuth compression

Fig. 7 n_{sp}=16, the profile of range and azimuth compression

(4 times interpolation)

When the up-sampling times is equal to 1, after echo signal with slant range approximation is compressed, the maximum

target's position offset is half of the sampling interval, which is shown in (a) of Fig.6. This position offset not only results in the main-lobe's stretch and the side-lobe's degradation of compressed signal in range direction, but also causes amplitude modulation of azimuth signal. So, it brings the reduced side-lobe peak and the poor resolution in azimuth direction. When the up-sampling times are equal to 16, after echo signal with slant range approximation is processed, the target's position offset is far less than half of the sampling interval. From Fig.7, it can be seen that the signal peak curves of range and azimuth compression with slant range approximation and with no approximation basically superpose. It indicates that the effect of slant range approximation on both range and azimuth compression can also be ignored when the interval of the adjacent equal range ring is equal to 1/16 of the sampling interval.

4 Simulation Analysis

4.1 The comparison of simulation speed

According to the simulation procedures of echo simulation algorithms including RTPC, IMIP and ESA–ES, the main operation quantities are estimated, which contributes to evaluate the speed of different echo algorithms. Here, they are characterized by the times of real multiplication and real addition.

The needed operation quantities of different echo algorithms are shown in Table 1. N_r, N_a is the sampling number of the simulated echo signal in range and azimuth dimension respectively, I_r, I_a represents the target number of natural scene in range and azimuth direction respectively, n_{sp} is the up-sampling times, N_f is the number of FFT (see Table 1).

Table 1 The computational quantities of different echo simulation algorithms

(normalized by $I_r \times I_a$ except the IMIP algorithm)

Echo algorithm	Times of real multiplication	Times of real addtition
RTPC	$10N_a$	$N_a \cdot N_r n_{sp}$
IMIP	$(N_a + N_r) \cdot (4N_f + N_f \log_2 N_f)$	$(N_a + N_r) \cdot (2N_f + 2N_f \log_2 N_f)$
ESA-ES	$10N_a$	$12N_a$

It can be seen from Table 1 that the speed of the ESA–ES algorithm is faster than that of the RTPC algorithm when there are large numbers of targets in the scene. Since the computational quantities of the IMIP algorithm are only related to the size of input image data, the efficiency of this algorithm is higher than that of the RTPC and ESA–ES algorithm.

Raw echo data of different target scenes is simulated using the RTPC, IMIP and ESA–ES algorithm. The simulation time is shown in Table 2. These echo algorithms are programmed by Matlab and run in PC (Personal Computer) with 2.8GHz CPU (Central Processing Unit) and 512MB RAM (Random Access Memory).

Table 2 The simulation time of different target scenes (s)

	RTPC	IMIP	ESA–ES
1×1(1309×1333)	11.40	14.7	22.3
128×128(1309×1333)	1740.9	14.82	78.6
512×512(1531×2401)	98332	30.24	1565.4

sFrom Table 2, it can be shown that the speed of the IMIP algorithm is the fastest, and the efficiency of the ESA–ES algorithm is higher than that of the RTPC algorithm with the increase of target number.

4.2 The comparison of simulation precision

(1) Point target simulation with error

The simulation parameters of point target are shown in Table 3. The sine velocity error is added along the motion direction of the platform, which is shown in Fig.8. The raw echo data of point target with sine error is generated using the RTPC, IMIP and ESA–ES algorithm respectively.

Table 3 The simulation parameters of point target

Simulation parameters	Value
Carrier frequency (GHz)	10
Signal Bandwidth (MHz)	150
Sampling rate (MHz)	200
Pulse width (us)	6
Pulse repetition frequency (Hz)	800
Azimuth resolution (m)	1
Interval of the adjacent equal range ring (m)	0.046875

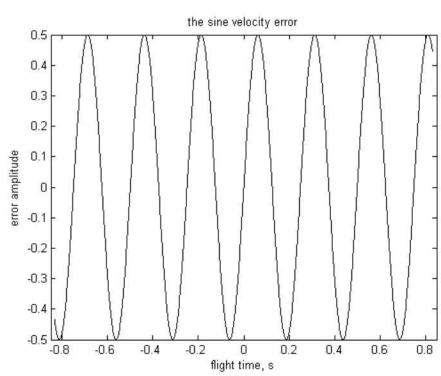

Fig. 8 The sine velocity error along the motion direction of the platform

In the echo domain, the correlation coefficient is used to characterize the similarity between the referenced and simulated echo signal. Its definition is

$$\rho = \frac{\left|\sum_u \sum_v s_1(u,v) s_2^*(u,v)\right|}{\sqrt{\sum_u \sum_v \left|s_1(u,v)\right|^2} \cdot \sqrt{\sum_u \sum_v \left|s_2(u,v)\right|^2}} \tag{21}$$

where $s_1(u,v)$ is the simulated echo signal, $s_2(u,v)$ is the referenced one.

Assumed that the echo signal simulated by a range time-domain addition (RTDA) algorithm is referred to as the referenced signal. The correlation coefficients between other three echo algorithms and the RTDA algorithm are computed. The simulation results are shown in Table 4.

Table 4 The correlation coefficients of point target's echo with error

	RTDA	RTPC	IMIP	ESA–ES
Correlation coefficient	1.0	0.9697	0.9150	0.9995

It can be seen from Table 4 that the correlation coefficient of the IMIP algorithm declines about 10% after the sine velocity error is added. However, the RTPC and ESA–ES algorithms are not basically affected by the time-variant velocity error. That is, the simulation precision of the IMIP algorithm becomes worse.

The point target's image parameters including the resolution, PSLR (Peak Side-lobe Ratio) and ISLR (Integrated Side-lobe Ratio) are measured after imaging processing. The simulation results are shown in Table 5.

Table 5 Point target's image parameters with error

	Resolution(m)		PSLR(dB)		ISLR(dB)	
	range	azimuth	range	azimuth	range	azimuth
RTDA	0.886	0.962	−13.31	−10.23	−9.83	−5.07
RTPC	0.888	0.962	−13.27	−10.23	−9.83	−4.99
IMIP	0.886	0.897	−13.29	−12.18	−9.82	−8.87
ESA-ES	0.886	0.963	−13.33	−10.23	−9.83	−5.08

The sine velocity error along the motion direction has an effect on azimuth compression, which mainly causes the degradation of the resolution, PSLR and ISLR. From Table 5, it can be shown that the measured parameters of point target's image using the RTDA, RTPC and ESA−ES algorithm in azimuth dimension become very poor, while those of the IMIP algorithm degrade a little. It illustrates that the IMIP algorithm is restricted by the time-variant velocity error, and the simulation precision of the algorithm is worse than that of other three echo algorithms.

(2) Natural scene simulation with error

The simulation parameters of natural scene are shown in Table 6. According to the point scattering model [3], the image data acquired by the flight experiment of a real airborne SAR with 360 × 240 pixels is regarded as targets' backscattering coefficients of natural scene. The different echo algorithms including RTDA, RTPC, IMIP and ESA−ES are used to generate natural scene's echo data with sine velocity error.

The correlation coefficients are measured in the echo domain. It can be seen from Table 7 that the correlation coefficient of the ESA−ES algorithm is very close to that of the RTDA algorithm. Yet, the correlation coefficient of the IMIP algorithm decreases about 50%, which indicates that the simulation precision of the IMIP algorithm is restricted by the sine vselocity error.

Table 6 The simulation parameters of natural scene

Simulation parameters	Value
Carrier frequency (GHz)	10
Signal Bandwidth (MHz)	150
Sampling rate (MHz)	200
Pulse width (us)	4
Pulse repetition frequency (Hz)	450
Azimuth resolution (m)	0.5
Interval of the adjacent equal range ring (m)	0.09375
Target number (pixel)	360×240

Table 7 The correlation coefficients of natural scene's echo with error

	RTDA	RTPC	IMIP	ESA−ES
Correlation coefficient	1.0	0.9662	0.4970	0.9985

Imaging processing is performed toward natural scene's echo data. The imaging results are shown in (a), (b) and (c) of Fig. 9 respectively.

The image quality of natural scene simulated by the RTDA, RTPC and ESA−ES algorithm is poor because the sine velocity error causes the pair-echoes affecting target's side-lobe level in azimuth dimension. However, it is difficult to add the time-variant velocity error in the IMIP algorithm. So, the quality of natural scene's image simulated by this algorithm is good from the angle of sight. It just illustrates that the simulation precision

of the IMIP algorithm is poor.

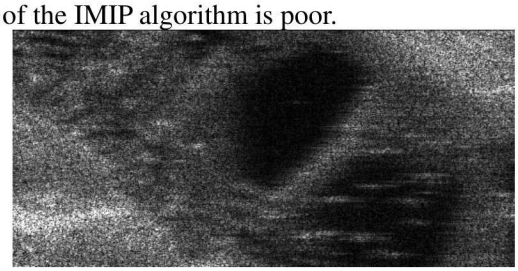

（a）The simulated image by RTPC

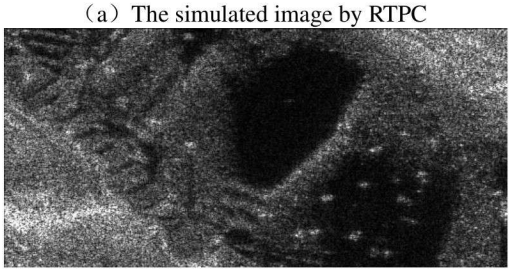

（b）The simulated image by IMIP

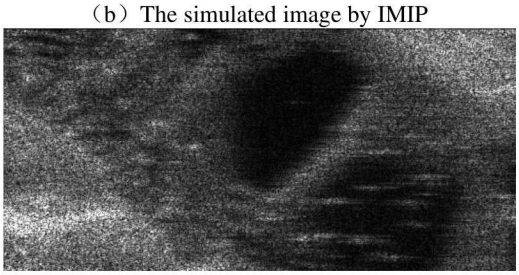

（c）The simulated image by ESA–ES

Fig. 9　The natural scene's image with error simulated by the RTPC, IMIP and ESA–ES algorithm

In the image domain, the image parameters are used to evaluate the performance of the simulated image. These parameters include the image's mean, the variance, the equivalent look number and the radiant resolution. Their definitions are as follows.

$$\mu_I = \frac{1}{IJ}\sum_{ii=1}^{I}\sum_{jj=1}^{J} g(ii, jj) \qquad (22)$$

$$\sigma_I^2 = \frac{1}{IJ}\sum_{ii=1}^{I}\sum_{jj=1}^{J}\left[g(ii, jj) - \mu_I \right]^2 \qquad (23)$$

$$M_{ENL} = \frac{\mu_I^2}{\sigma_I^2} \qquad (24)$$

$$\gamma_e = 10\lg\left(\frac{1}{\sqrt{M_{ENL}}} + 1\right) = 10\lg\left(\frac{\sigma_I}{\mu_I} + 1\right) \qquad (25)$$

where μ_I is the image's mean, σ_I^2 is the image's variance, M_{ENL} is the equivalent look number and γ_e is the radiant resolution. $I \times J$ is the pixel number of SAR image, and $g(ii, jj)$ is the gray of the (ii, jj) pixel.

The parameters of natural scene's image simulated by different echo algorithms including RTDA, RTPC, IMIP and ESA–ES are measured, which are shown in Table 8.

Table 8　The normalized image parameters of natural scene with error

	Image mean	Image variance	Equivalent look number	Radiant resolution(dB)
RTDA	0.0782	0.0059	1.0356	2.9724
RTPC	0.0757	0.0055	1.0361	2.9719
IMIP	0.0628	0.0044	0.9010	3.1250
ESA-ES	0.0784	0.0059	1.0384	2.9696

It can be shown from Table 8 that the measured parameters of natural scene's image simulated by the RTPC and ESA–ES algorithm are very close to those of the RTDA algorithm, while they are different from those of the IMIP algorithm. It also implies that the simulation precision of the IMIP algorithm is worse than that of other three echo simulation algorithms when the sine velocity error exists.

5　Summary

The echo simulation algorithm in terms of equivalent scatterer is proposed as to raw echo data simulation of SAR. On the basis of establishing the coordinate system of slant plane, the signal model of the algorithm is deduced, the simulation procedures are given,

as well as the effect of slant range approximation on echo simulation and imaging processing are analyzed from the viewpoint of error in detail.

The performance differences of different echo simulation algorithms including RTPC, IMIP and ESA–ES are drawn a comparison between the computation quantities and the simulation precision. The simulation speed of the IMIP algorithm is the fastest, the speed of the ESA–ES algorithm is the second, and that of the RTPC algorithm is the third. When the sine velocity error is added along the motion direction of the platform, the fidelity of the ESA–ES and RTPC algorithm is better than that of the IMIP algorithm.

Through numerical simulation of point target and natural scene, it is indicated that the ESA-ES algorithm can not only generate raw data fast, but ensure the simulation precision of echo data when SAR system contains the time-variant motion error. As a conclusion, it is significant to investigate the efficiency and the evaluation method of natural scene's raw data simulation in order to meet the requirement of engineering research.

References

[1] Franceschetti G., Migliaccio M., Riccio D., and Schirinzi G.: 'SARAS: a synthetic aperture radar (SAR) raw signal simulator', IEEE Trans. Geosci. Remote Sensing, 1992, 30 (1): 110—123

[2] Franceschetti G., Migliaccio M., and Riccio D.: 'SAR raw signal simulation of actual ground sites described in terms of sparse input data', IEEE Trans. Geosci. Remote Sensing, 1994, 32 (2): 1160—1169

[3] Holtzman J.C., Frost V.S., Abbott J.L., and Kaupp V.H.: 'Radar image simulation', IEEE Trans. Geosci. Remote Sensing, 1978, 16 (4): 296—303

[4] Pike T.K.: 'SARSIM: A synthetic aperture radar system simulation model', DFVLR-Mitt, 1985

[5] Shunsheng Zhang, Teng Long, Tao Zeng, and Zegang Ding: 'Space-borne synthetic aperture radar received data simulation based on airborne SAR image data', Advances in Space Research, 2008, 41 (11): 1818—1821

[6] Liu Yongtan: 'SAR imaging' (in Chinese), Harbin Institute of Technology Press, 1999

[7] Li Linjie, Wang Jianguo, and Huang Shunji: 'SAR raw-data simulation based on real reflection-field SAR images' (in Chinese), Journal of UEST of China, 1996, 25 (6): 566—568

[8] Yu Ming-cheng, Xu Jia, Peng Ying-ning, and Wang Xiu-yun: 'Fast simulation of SAR raw signal' (in Chinese), Journal of System Simulation, 2006, 18(12); 122—125

[9] Curlander J.C., and McDonough R.H.: 'Synthetic aperture radar: systems and signal processing', John Wiley & Sons, Inc. New York, 1991

[10] Thomas L.M., Elizabeth A.M, and Charles P.P.: 'Fast pulse Doppler radar processing accounting for range bin migration', IEEE National Radar Conference, 1993: 264—266

[11] Bamler R.: 'A comparison of range-Doppler and wavenumber domain SAR focusing algorithms', IEEE Trans. Geosci. Remote Sensing, 1992, 30 (4): 706—713